A mitochondrial carrier transports glycolytic intermediates to link cytosolic and mitochondrial glycolysis in the human gut parasite *Blastocystis*

Eva Pyrihová[1,2], Martin S. King[1], Alannah C. King[1], M. Rey Toleco[2], Mark van der Giezen[2]* and Edmund R.S. Kunji[1]*

[1]Medical Research Council Mitochondrial Biology Unit, The Keith Peters Building, Cambridge Biomedical Campus, Hills Road, Cambridge, CB2 0XY, United Kingdom.

[2]University of Stavanger, Department of Chemistry, Bioscience, and Environmental Engineering, Richard Johnsens gate 4, N-4021 Stavanger, Norway.

*Authors to whom correspondence should be addressed

Tel.: +47 5183 4493, e-mail: mark.vandergiezen@uis.no

Tel.: + 44 1223 252850, e-mail: ek@mrc-mbu.cam.ac.uk

Key words

Bioenergetics, SLC25 mitochondrial carrier family, missing transport link, carboxylate carriers, thermostability shift assays, transport assays, anaerobic and aerobic metabolism, protists, parasites.

Abstract

Stramenopiles form a clade of diverse eukaryotic organisms, including multicellular algae, the fish and plant pathogenic oomycetes, such as the potato blight *Phytophthora,* and the human intestinal protozoan *Blastocystis*. In most eukaryotes, glycolysis is a strictly cytosolic metabolic pathway that converts glucose to pyruvate, resulting in the production of NADH and ATP. In contrast, stramenopiles have a branched glycolysis in which the enzymes of the pay-off phase are located in both the cytosol and the mitochondrial matrix. Here, we identify a mitochondrial carrier in *Blastocystis* that can transport glycolytic intermediates, such as dihydroxyacetone phosphate and glyceraldehyde-3-phosphate, across the mitochondrial inner membrane, linking the cytosolic and mitochondrial branches of glycolysis. Comparative analyses with the phylogenetically-related human mitochondrial oxoglutarate carrier (SLC25A11) and dicarboxylate carrier (SLC25A10) show that the glycolytic intermediate carrier has lost its ability to transport the canonical substrates malate and oxoglutarate. *Blastocystis* lacks several key components of oxidative phosphorylation required for the generation of mitochondrial ATP, such as complexes III and IV, ATP synthase and ADP/ATP carriers. The presence of the glycolytic pay-off phase in the mitochondrial matrix generates ATP, which powers energy-requiring processes, such as macromolecular synthesis, as well as NADH, used by mitochondrial complex I to generate a proton motive force to drive the import of proteins and molecules. Given its unique substrate specificity and central role in carbon and energy metabolism, the carrier for glycolytic intermediates identified here represents a specific drug and pesticide target against stramenopile pathogens, which are of great economic importance.

Introduction

Glycolysis is a crucial metabolic pathway that most organisms use to obtain energy from the oxidation of sugars, which consists of ten enzymatic reactions in total, divided into two phases. The first 'preparatory' phase consists of five reactions, the products of which are the triose phosphates dihydroxyacetone phosphate and glyceraldehyde-3-phosphate. The second 'pay-off' phase leads to the production of ATP, NADH and pyruvate, which is transported into the mitochondrial matrix by the mitochondrial pyruvate carrier (Bricker et al., 2012; Herzig et al., 2012). In most eukaryotes, glycolysis is a cytosolic process with the exception of trypanosomes, where it is localised in the glycosomes (Opperdoes and Borst, 1977). However, it was recently discovered that a large group of eukaryotes, the stramenopiles, have a branched glycolytic pathway in which the pay-off phase is duplicated and also localised in mitochondria (Abrahamian et al., 2017; Bártulos et al., 2018). The stramenopiles are an extremely diverse eukaryotic group consisting mainly of protist algae, which are among the most important primary oxygen producers in the oceans (Burki et al., 2020). The group also includes multicellular algae (kelps) and the economically-devastating oomycetes, such as *Phytophthora infestans* (Jiang and Tyler, 2012), which causes potato blight, one of the major contributing factors of the Great Famine in Ireland in the late 19th century.

The human gut protozoan *Blastocystis* also belongs to the stramenopiles. Despite more than one billion infected individuals worldwide (Andersen and Stensvold, 2016), the public health significance of *Blastocystis* is debated. *Blastocystis* is often linked to patients with diarrhoea, irritable bowel syndrome (Poirier et al., 2012), or inflammatory bowel disease (Dogruman-Al et al., 2009). However, it is also frequently found in healthy individuals, and a few microbiome studies associated *Blastocystis* with higher microbial diversity (Andersen et al., 2015; Audebert et al., 2016; Stensvold et al., 2022). The controversy may arise from the extreme genetic diversity of *Blastocystis*, which is classified into over 40 subtypes (Andersen et al., 2015; Stensvold et al., 2023), and thus its influence on gut microbiota is likely to be subtype-specific (Tito et al., 2019). Nevertheless, *Blastocystis* ST7-B, which was used in this study, is most frequently associated with pathogenic phenotypes (Ajjampur et al., 2016; Deng et al., 2023; Stensvold et al., 2009; Wu et al., 2014; Yason et al., 2019) and was recently linked to a decreased microbial diversity in

diarrheal patients (Deng et al., 2022). The treatment of choice is metronidazole (Stenzel and Boreham, 1996), but there have been reports of resistance (Haresh et al., 1999; Mirza et al., 2011; Moghaddam et al., 2005), highlighting the need for new therapeutic interventions.

Unlike other stramenopiles, *Blastocystis* has lost the cytosolic pay-off phase of glycolysis, consistent with the absence of a gene encoding a mitochondrial pyruvate carrier (Bártulos et al., 2018). The only exception is the last enzyme of the pathway, pyruvate kinase, which was also identified as a cytosolic protein (Lantsman et al., 2008). *Blastocystis* is an anaerobe (Zierdt, 1991) with highly divergent mitochondria (Stechmann et al., 2008). It has respiratory complexes I and II, but lacks the rest of the electron transport chain, as well as ATP synthase and mitochondrial ADP/ATP carriers (Gentekaki et al., 2017; Stechmann et al., 2008; Wawrzyniak et al., 2008). Therefore, *Blastocystis* relies mainly on glycolysis and fermentation for its metabolic energy requirements (Müller et al., 2012). The transport of glycolytic intermediates across the mitochondrial inner membrane is necessary for the completion of glycolysis and is critical for the survival of the parasite. Glycolytic enzymes are powerful drug targets in parasites that are strictly dependent on glycolysis for ATP production. The structural differences between host and parasitic glyceraldehyde-3-phosphate dehydrogenase and triosephosphate isomerase in *Plasmodium falciparum* have been studied with the aim of inhibiting glycolysis (Bruno et al., 2014; Penna-Coutinho et al., 2011; Ravindra and Balaram, 2005). Similarly, inhibitors against phosphofructokinase in *Trypanosoma brucei* have a rapid effect on the parasite viability without inhibiting the host enzyme (McNae et al., 2021). Understanding the unique aspects of parasite metabolism is crucial for the discovery of new drug targets.

It is clear that the branched stramenopile glycolysis needs to be linked by a specific transporter in the mitochondrial inner membrane, as the solute exchange between the cytosol and mitochondrial matrix is tightly controlled (Kunji et al., 2020; Ruprecht and Kunji, 2020). The mitochondrial carrier family (SLC25) is the largest solute transporter family in humans (Kunji et al., 2020). Its members facilitate the transport of nucleotides, amino acids, inorganic ions, keto acids, vitamins and other nutrients across the mitochondrial inner membrane. All SLC25 members have a three-fold

pseudo-symmetric structure, evident at the sequence level by the presence of three conserved homologous repeats (Saraste and Walker, 1982) and specific motifs important for their transport mechanism (Ruprecht et al., 2019; Ruprecht and Kunji, 2020, 2021).

Here, we report a stramenopile-specific group of transport proteins closely related to mitochondrial carboxylate carriers of the SLC25 family. We characterised one of these unique *Blastocystis* carriers, which has lost its ability to transport the canonical substrates malate and oxoglutarate. Instead, this carrier can transport several glycolytic intermediates, including dihydroxyacetone phosphate, glyceraldehyde-3-phosphate, 3-phosphoglycerate and phosphoenolpyruvate, thus providing a previously undiscovered transport link between cytosolic and mitochondrial glycolysis. Since *Blastocystis* relies solely on mitochondrial glycolysis, the inhibition of this carrier might represent a promising way to treat this parasite.

Results

A group of mitochondrial carboxylate carriers that is unique to stramenopiles

The last enzyme of the cytosolic phase of glycolysis in *Blastocystis* is triosephosphate isomerase (Bártulos et al., 2018). Consequently, dihydroxyacetone phosphate and glyceraldehyde-3-phosphate need to be transported into the mitochondrial matrix for the pay-off phase of glycolysis. Given the presence of mitochondrial glycolysis in stramenopiles, we searched for a transporter that is not only ubiquitous in stramenopiles, but also absent in other eukaryotes. As glycolysis in *Blastocystis* would be critically dependent on this transporter, we used this parasite as a model organism. We focused on mitochondrial carboxylate carriers because of their ability to transport phosphorylated three-carbon substrates (Castegna et al., 2010; Fiermonte et al., 2001; Palmieri et al., 1972) and compared the sequences of carboxylate carriers from all major eukaryotic supergroups. Our analyses revealed four well-defined groups of carriers: dicarboxylate carriers (DIC, SLC25A10), oxoglutarate/malate carriers (OGC, SLC25A11), di/tricarboxylate carriers (DTC), and a new stramenopile-specific group, the putative glycolytic intermediate carriers (GIC) (**Figure 1**). At least one copy of the putative GIC carrier was identified in each stramenopile species. In *Blastocystis* ST7-B, there are four copies of the putative GIC protein, but two of them are truncated and lack crucial mitochondrial carrier

elements (Ruprecht et al., 2019; Ruprecht and Kunji, 2020, 2021), possibly rendering these proteins non-functional (XP_012899519.1 has an N-terminal truncation; XP_012896318.1 has a C-terminal truncation) (Ruprecht and Kunji, 2020).

The unidentified *Blastocystis* carriers localise to mitochondria

Another important criterion is that the putative glycolytic intermediate carriers localise to mitochondria in *Blastocystis*. Specific (peptide) rabbit antibodies were raised against the two putative glycolytic intermediate carriers bGIC-1 and bGIC-2 as well as an ortholog of the *Blastocystis* oxoglutarate carrier bOGC (**Figure 2B**). Mitochondria were visualized using antibodies raised against a triosephosphate isomerase/glyceraldehyde-3-phosphate dehydrogenase mitochondrial fusion protein (TPI-GAPDH) (Bártulos et al., 2018). Immunoconfocal microscopy clearly show that bOGC, bGIC-1 and bGIC-2 localise to mitochondria in *Blastocystis*, showing that they are potential candidates for the missing transport links (**Figure 2A**).

Human and *Blastocystis* carriers purified from yeast mitochondria are folded

All three *Blastocystis* proteins were expressed in and purified from *Saccharomyces cerevisiae* mitochondria using the detergent lauryl maltose neopentyl glycol (**Figure 3A**). They were compared to the human oxoglutarate carrier SLC25A11 (hOGC) and dicarboxylate carrier SLC25A10 (hDIC), prepared in the same way. Next, thermostability analysis was used to assess whether the purified proteins are correctly folded. Spectral properties of tryptophan/tyrosine residues change as their local environment changes during protein denaturation in a temperature ramp (Alexander et al., 2014). The assay produces an apparent melting temperature (Tm) at which the rate of protein unfolding is the highest. All three proteins produced unfolding curves, showing that they are folded. The apparent melting temperatures for bOGC (52.6 ± 0.5 °C), bGIC-1 (60.7 ± 0.4 °C) and bGIC-2 (59.8 ± 0.4 °C) (**Figure 3B** and **C**) are similar to those observed for hOGC (51.0 °C), hDIC (54.1 °C) and other mitochondrial carriers (Crichton et al., 2015; Jaiquel Baron et al., 2021; Majd et al., 2018).

Two mitochondrial carriers of *Blastocystis* bind glycolytic intermediates

We have previously shown that inhibitors (Crichton et al., 2015; Jaiquel Baron et al., 2021; Tavoulari et al., 2022) and substrates (Majd et al., 2018; Mavridou et al., 2022)

can specifically stabilize a population of transport proteins in thermal denaturation assays. This technique provides a simple, high-throughput method for screening libraries of compounds to identify potential protein binders that can then be confirmed in low-throughput transport assays with radiolabelled substrates (Majd et al., 2018). We used detergent-solubilized, purified protein to screen a library of 39 commercially available compounds, which included mono-, di- and tricarboxylates, acids, inorganic ions, and several glycolytic intermediates (with the exception of 1,3-bisphosphoglycerate and 2-phosphoglycerate, which were not available).

In order to quantify the binding effect of a compound, we calculated a thermostability shift (ΔTm) by subtracting the apparent melting temperature in the absence of a compound from that in its presence. A positive shift suggests that the compound is stabilizing, indicating a putative substrate (Majd et al., 2018). We first tested the library on purified hOGC (SLC25A11) and hDIC (SLC25A10). A range of compounds had stabilizing effects on hOGC in thermostability shift assays (**Figure 4A**). Oxoglutarate (3.8 ± 0.4 °C), malate (3.6 ± 0.3 °C), maleate (3.1 ± 0.1 °C), succinate (1.9 ± 0.3 °C) and malonate (1.3 ± 0.2 °C) all produced positive shifts. For hDIC, larger shifts than for hOGC were observed for malate (4.8 ± 0.2 °C), maleate (8.0 ± 0.1 °C), succinate (3.0 ± 0.3 °C) and malonate (7.3 ± 0.1 °C) (**Figure 4B**). Shifts were also observed for sulphate (3.0 ± 0.2 °C), thiosulphate (4.0 ± 0.4 °C), phosphate (3.2 ± 0.2 °C), dihydroxyacetone phosphate (2.5 ± 0.4 °C) and glyceraldehyde-3-phosphate (5.6 ± 0.6 °C) (**Figure 4B**), which were not observed for hOGC and may reflect a difference in substrate specificity (Crompton et al., 1974).

The thermostability shifts for the *Blastocystis* ortholog bOGC were similar to those of hOGC (SLC25A11), although some compounds, most notably citrate and isocitrate, produced small stabilizations that were not observed for the human ortholog (**Figure 4C**). A wider range of compounds caused an increase in stability of the two candidate carriers bGIC-1 and bGIC-2 compared to bOGC (**Figure 4D** and **E**). These compounds included glycolytic intermediates, such as glyceraldehyde-3-phosphate (1.0 ± 0.1 °C and 2.1 ± 0.1 °C for bGIC-1 and bGIC-2, respectively) and dihydroxyacetone phosphate (3.6 ± 0.2 °C and 1.6 ± 0.1 °C) and inorganic ions, such as phosphate (1.7 ± 0.1 °C and 5.0 ± 0.1 °C) and sulphate (2.3 ± 0.2 °C and 2.6 ± 0.3

°C). A significant shift was observed for phosphoenolpyruvate (PEP) in the case of bGIC-2 (4.3 ± 0.2 °C). In comparison, hOGC showed no shift for any of these compounds (**Figure 4A**), whereas bOGC showed only a minor shift in the presence of sulphate (0.5 ± 0.1 °C) (**Figure 4C**).

Human OGC and DIC have distinct and overlapping substrate specificities

In addition to the glycolytic intermediates that were the focus of this study, we selected all compounds that stabilized the proteins in thermostability assays and performed transport assays. To test whether a compound was transported, we loaded proteoliposomes with substrate by freeze-thaw-extrusion (Jaiquel Baron et al., 2021), and initiated exchange with the addition of radiolabelled [^{14}C]-malate (hOGC and bOGC, **Figure 3D** and **E**) or [^{35}S]-sulphate (hDIC). Only when the internalized compound is a transported substrate of the carrier will the uptake of radiolabelled substrate occur. For hOGC (SLC25A11), uptake was measured for oxoglutarate, oxaloacetate, malate, succinate, maleate, malonate, 2-oxoadipate (**Figure 5A**). Surprisingly, a low uptake rate was measured for pyruvate, which did not induce a significant shift (0.1 ± 0.3 °C). Pyruvate is a small molecule and therefore probably does not introduce enough additional bonds to stabilize the protein. The substrate specificity of hOGC is similar to that of the rat and bovine oxoglutarate carrier (Bisaccia et al., 1988; Fiermonte et al., 1993; Palmieri et al., 1972). For hDIC (SLC25A10), uptake was observed for malate, succinate, maleate, malonate, sulphate, thiosulphate, phosphate and, to a lesser extent, oxalic acid and dihydroxyacetone phosphate (**Figure 5B**). This result is consistent with previous data that have shown that the rat dicarboxylate carrier also transports sulphate and thiosulphate in addition to dicarboxylates (Crompton et al., 1974; Saris, 1980). Although we measured transport for dihydroxyacetone phosphate, we have not found any evidence for the presence of dihydroxyacetone phosphate inside mitochondria in the literature. It is possible that it is not transported under physiological conditions in competition with dicarboxylates or other substrates. The substrate specificity of *Blastocystis* OGC (**Figure 5C**) is very similar to human OGC (**Figure 5A**), consistent with their close phylogenetic relationship.

***Blastocystis* GIC-2 links cytosolic and mitochondrial glycolysis**

We first tested [^{14}C]-malate/malate homo-exchange for bGIC-1 and bGIC-2 (**Figure 6A** and **B**, respectively). No transport was measured, showing that these proteins do not have the ability to transport malate. We next aimed to find a radiolabelled substrate that is transported by bGIC-1 and bGIC-2. We tested [^{33}P]-phosphate/phosphate and [^{35}S]-sulphate/sulphate homo-exchange, as both of these compounds induce relatively large shifts in thermostability assays: bGIC-1 (1.7 ± 0.1 °C and 2.3 ± 0.2 °C) and bGIC-2 (5.0 ± 0.1 °C and 2.6 ± 0.3 °C), for phosphate and sulphate, respectively (**Figure 4D** and **E**). No transport was detected for either phosphate (**Figure 6C**) or sulphate (**Figure 6E**) for bGIC-1. In contrast, bGIC-2 showed transport activity for both: the rate of [^{33}P]-phosphate/phosphate homo-exchange was 4.5 times above the background (**Figure 6D**), and the rate of [^{35}S]-sulphate/sulphate homo-exchange was 22 times above background (**Figure 6F**). We, therefore, used [^{35}S]-sulphate as a counter-substrate and tested hetero-exchange to determine the substrate specificity of bGIC-2 (**Figure 5D**). No transport was observed for the canonical oxoglutarate carrier substrates, including oxaloacetate, malate, succinate and 2-oxoadipate; oxoglutarate, maleate and malonate displayed only low transport rates. Interestingly, bGIC-2 displayed high transport rates for phosphate, sulphate, and thiosulphate and for the glycolytic intermediates dihydroxyacetone phosphate, glyceraldehyde-3-phosphate, 3-phosphoglycerate and phosphoenolpyruvate (**Figure 5D**).

Discussion

Glycolysis is a textbook example of a well-conserved cytosolic pathway. However, the discovery that glycolysis is branched and also mitochondrial in stramenopiles (Abrahamian et al., 2017; Bártulos et al., 2018; Nakayama et al., 2012) raises questions about how glycolytic intermediates are transported across the tightly controlled mitochondrial inner membrane. Here, we report the discovery and characterisation of a mitochondrial carrier protein unique to stramenopiles that transports the glycolytic intermediates dihydroxyacetone phosphate, glyceraldehyde-3-phosphate and phosphoenolpyruvate, providing the heretofore missing transport link.

Since mitochondrial glycolysis is found exclusively in stramenopiles, we searched for a transporter that is ubiquitous in these species, but not in other eukaryotes. Phylogenetic analyses identified a new class of mitochondrial carboxylate carriers in stramenopiles that are most closely related to plant di/tricarboxylate carriers (**Figure 1**). The plant carriers catalyse the transport of tricarboxylates (citrate, isocitrate, and aconitate) in exchange for dicarboxylates (oxoglutarate, oxaloacetate, malate, maleate, succinate, and malonate) (Picault et al., 2002) and are also present in Alveolata, Rhizaria, and Haptophyta (Toleco et al., 2020), which share a common evolutionary ancestor with stramenopiles (Burki et al., 2020). Therefore, the glycolytic intermediate carrier of stramenopiles is probably derived from a common ancestor with di/tricarboxylate carriers and does not exist in any other eukaryote outside of the stramenopile clade.

Blastocystis was used in this study as a stramenopile model organism, as it relies solely on glycolysis for its energy demands and does not have a second branch of glycolysis in the cytosol. We characterised human and *Blastocystis* carboxylate carriers and demonstrated that the stramenopile GIC proteins have a unique substrate specificity that is distinct from the human carriers (**Figure 5**). We also characterised the substrate specificity of *Blastocystis* OGC, which has the same specificity as human OGC (SLC25A11), and we demonstrated that it is unable to transport glycolytic intermediates and thus could not be the missing transport step in the branched glycolytic pathway.

Blastocystis GIC-1 did not transport any of the tested substrates (**Figure 6A**, **C** and **E**), but it is expressed and localised to mitochondria (**Figure 2**), demonstrating that it is not a pseudogene. We did not test radiolabelled glycolytic intermediates directly in transport, as phosphoenolpyruvate and dihydroxyacetone phosphate are not available, and radiolabelled glyceraldehyde-3-phosphate is prohibitively expensive. We cannot, therefore, exclude the possibility that GIC-1 catalyses glycolytic intermediate exchange, but not in hetero-exchange reactions with malate, phosphate and sulphate. It is more likely that bGIC-1 has lost its transport activity and could possibly fulfil a different role. For example, in *Tetrahymena thermophila*, a non-functional OGC-like carrier is incorporated into a respiratory supercomplex (Zhou et al., 2022). In contrast to bGIC-1, bGIC-2 transports several inorganic ions and

glycolytic intermediates, including dihydroxyacetone phosphate and glyceraldehyde-3-phosphate (**Figure 5D**), but not the canonical substrates of *Blastocystis* OGC, such as malate, maleate, malonate, and succinate. Most mitochondrial carriers operate as strict antiporters, where the chemical gradient of one substrate drives the uptake of the counter-substrate (Ruprecht and Kunji, 2020). A mitochondrial phosphate carrier homolog was identified in the phylogenetic analysis of *Blastocystis* (**Figure 1 - figure supplement 1**), which is driven by the proton motive force to maintain high concentrations of phosphate in the mitochondrial matrix, which in turn could drive the uptake of glycolytic intermediates. *Blastocystis* lacks many of the conserved carrier proteins found in the mitochondria of aerobes. In total, we have only identified 18 mitochondrial carriers in *Blastocystis* (**Figure 1 - figure supplement 1**). However, we show that bGIC-2 seems to be able to compensate for the loss of some mitochondrial carriers, including the transport of inorganic ions in the absence of a DIC homolog. Additionally, the distantly related citrate carrier, which transports dicarboxylates, tricarboxylates and PEP, was also lost in *Blastocystis*, possibly due to an incomplete TCA cycle devoid of citrate synthase, aconitase, isocitrate dehydrogenase and α-ketoglutarate dehydrogenase (Stechmann et al., 2008; Zierdt et al., 1988). In *Blastocystis*, PEP can be synthesised from mitochondrial pyruvate via oxaloacetate (Gentekaki et al., 2017; Stechmann et al., 2008), and here we show that PEP transport is catalysed by bGIC-2. When PEP is exported by bGIC-2, it could be converted into pyruvate and lactate by cytosolic pyruvate kinase and lactate dehydrogenase, respectively (Lantsman et al., 2008), which would lead to the synthesis of ATP and the conversion of NADH to NAD^+ in the cytosol. This reaction may play a significant role in cytosolic ATP generation, as there is no mitochondrial ADP/ATP carrier in *Blastocystis* for adenine nucleotide exchange (**Figure 1 - figure supplement 1**). *Blastocystis* also contains a glycerol-3-phosphate dehydrogenase (Gentekaki et al., 2017), which oxidises NADH to convert glycerol-3-phosphate to dihydroxyacetone phosphate, which in turn can be transported into mitochondria by bGIC-2 to generate ATP and reducing equivalents. In most other eukaryotes, cytosolic NADH is oxidised by the malate-aspartate shuttle, but this pathway requires an ortholog of the mitochondrial aspartate/glutamate carrier, which could not be identified in *Blastocystis*, even though it might have a mitochondrial glutamate carrier (**Figure 1 - figure supplement 1**).

What selective advantage could there be to have the pay-off phase of glycolysis in the mitochondrial matrix? *Blastocystis* is well adapted to an anoxic environment with its anaerobic metabolism but has a limited ability to detoxify oxygen. In its natural environment, *Blastocystis* likely uses protons as terminal electron acceptors by using pyruvate:ferredoxin oxidoreductase, which would result in the production of hydrogen and a range of fermentative products, such as lactate, acetate, and propionate (Gentekaki et al., 2017; Lantsman et al., 2008; Stechmann et al., 2008). Under aerobic stress, such as in a dysbiotic gut (Stensvold and van der Giezen, 2018), it possibly uses oxygen as the terminal electron acceptor by using alternative oxidase, which produces water (Tsaousis et al., 2018). However, as a likely adaptation to the anoxic environment, *Blastocystis* has lost some of the canonical components of oxidative phosphorylation, including complexes III and IV of the respiratory chain, ATP-synthase and mitochondrial ADP/ATP carriers (Stechmann et al., 2008). Consequently, it has lost its ability to synthesize mitochondrial ATP via this route. This role was taken over by transfer of the pay-off phase of glycolysis to the mitochondrial matrix in *Blastocystis*, which has several advantages. The degradation of one glucose molecule in the cytosol requires one ATP and one pyrophosphate molecule, but will generate four ATP molecules in the mitochondrial matrix, which can be used for ATP-requiring processes, such as protein import, mitochondrial DNA replication and transcription, and mitochondrial protein synthesis (Denoeud et al., 2011; Gentekaki et al., 2017). In addition, two NAD^+ molecules are reduced to NADH, which can be used by complex I to generate a proton motive force to drive the import of proteins and the uptake of ions and molecules into mitochondria, such as phosphate. Cytosolic ATP can be supplied either through the export of PEP by bGIC-2, as explained, or via a mitochondrial carrier that shares properties with the mitochondrial Mg-ATP/Pi carrier, which is generally used to equilibrate adenine nucleotide pools between the matrix and cytosol.

Our results show that the canonical metabolic pathways studied in common model organisms can be altered in non-model eukaryotic species (**Figure 7**). Moreover, the newly discovered glycolytic intermediates carrier demonstrates the plasticity of mitochondrial carriers in terms of their substrate specificity. Through the discovery of this carrier, we have linked the two halves of glycolysis and provided a potential

target for specific treatment not only for *Blastocystis* but also for other stramenopile pathogens that threaten global food security.

Materials and Methods

In-silico analysis

Bioinformatics-based approaches were used to identify potential candidates for a glycolytic intermediate transporter. Any potential transporter should be present in all stramenopiles, but absent in other eukaryotes, and could plausibly transport phosphorylated three carbon substrates. Most of the transport proteins in mitochondria belong to the mitochondrial carrier family (SLC25) (Kunji et al., 2020; Ruprecht and Kunji, 2020), and thus the initial search focused on them.

Mitochondrial carrier sequences were gathered using 53 human mitochondrial carriers as a BLAST query against the genomes of selected stramenopiles: *Blastocystis* ST7-B*, Aureococcus anophagefferens, Ectocarpus sp.*, *Saprolegnia parasitica, Phaeodactylum tricornutum* and *Phytopthora infestans*. InterProScan (www.ebi.ac.uk/interpro/search/sequence/) was then used to discard non-carrier hits (Jones et al., 2014), and partial sequences were removed (sequences with fewer than three signature repeats or 250 amino acids). Reciprocal BLAST was then used to eliminate incorrectly assigned sequences. The stramenopile sequences were aligned to *Homo sapiens, Saccharomyces cerevisiae* and *Arabidopsis thaliana* carriers. To prepare the alignment for phylogenetic analysis, the structures of the ADP/ATP carrier (PDB: 1OKC and 6GCI) were used to identify and remove the hypervariable loop regions in each sequence.

IQ-TREE was used to calculate a phylogenetic tree using an LG + F + R9 model suggested by ModelFinder and branch supports were generated by ultrafast bootstrap with 1000 replicates (Hoang et al., 2018; Minh et al., 2020). A clade of stramenopile-specific transporters was identified as a sister group to the *A. thaliana* di/tricarboxylate carrier homologs (DTC) (**Figure 1 - figure supplement 1**). Within this clade, all selected stramenopile species were represented at least once. Interestingly, *Blastocystis,* which has no homolog of the mitochondrial pyruvate carrier, and would have to rely solely on the import of glycolytic intermediates, has four copies of this carrier. Given that DTC substrates are three-carbon dicarboxylates

and tricarboxylates, it is possible that a closely related carrier could transport phosphorylated three-carbon substrates.

To investigate whether this clade is not only present in stramenopiles, but also unique to them, BLAST searches were performed using the unique stramenopile sequences against genomes from an expanded range of eukaryotes using NCBI and EukProt databases (Priyam et al., 2019). The collected sequences were screened to remove partial and duplicate sequences and sequences that shared contact points with carboxylate carriers (Kunji and Robinson, 2006; Robinson and Kunji, 2006) were selected. They were added to a multiple sequence alignment of the identified stramenopile carriers and other closely related transporters from the first tree. The maximum likelihood tree was generated by IQ-TREE with the LG + F + R7 model suggested by ModelFinder (Minh et al., 2020). Branch supports were generated by ultrafast bootstrap with 1000 replicates (Hoang et al., 2018).

To address the absence of GIC in other species and exclude the possibility of its presence outside of stramenopiles, we performed additional analyses. The stramenopile GIC sequences were blasted against NCBI datasets encompassing major eukaryotic groups, and the top hits were selected and aligned with GIC sequences. Phylogenetic analysis of this expanded dataset revealed that the non-stramenopile carriers are more closely related to other carboxylate carriers, indicating that even the carriers most similar to GIC do not fall within the GIC clade. These analyses confirmed that the putative GIC carriers are universal in stramenopiles and also unique to them.

Protein production in mitochondria of *Saccharomyces cerevisiae*

Genes (SLC25A11, the human oxoglutarate carrier (hOGC), UniProt accession code: Q02978; SLC25A10, the human dicarboxylate carrier (hDIC), UniProt accession code: Q9UBX3; *Blastocystis* ST7-B oxoglutarate carrier (bOGC) UniProt accession code: D8M7L1; *Blastocystis* ST7-B potential glycolytic intermediate carrier 1 (bGIC-1), UniProt accession code: D8LYZ6; *Blastocystis* ST7-B potential glycolytic intermediate carrier 2 (bGIC-2), UniProt accession code: D8LWW2) were codon-optimized with N-terminal eight histidine tag and a Xa protease cleavage site to aid purification (hOGC, Δ2-13; hDIC, GKP added (positions 2-4); bGIC-1, Δ2-3; bGIC-2,

Δ2). The modified genes were cloned into a pYES2/CT vector (Invitrogen) under the control of an inducible galactose promoter, as previously described (King and Kunji, 2020), and expressed in *Saccharomyces cerevisiae* (GenScript) strain W303.1B (hOGC and bGIC-2) or the protease-deficient strain BJ2186 (hDIC, bOGC and bGIC-1). Transformants were selected on Sc-Ura + 2 % (w/v) glucose plates. For large-scale expression, a pre-culture of cells grown in Sc-Ura + 2% (w/v) glucose was inoculated into 50 L of YPG plus 0.1% glucose medium in an Applikon Pilot Plant 140 L bioreactor. Cells were grown at 30 °C for 20 hours, induced with a final concentration of either 0.4% (hOGC, hDIC and bGIC-1) or 2.0% (bOGC and bGIC-2) galactose, grown for a further 4 (hOGC) or 8 hours (hDIC, bOGC, bGIC-1 and bGIC-2), and harvested by centrifugation (4,000 *g*, 20 minutes, 4 °C). Alternatively, 15 L of culture were grown in shaker flasks and induced as above. Crude mitochondria were prepared using a bead mill (Dyno-Mill Multilab, Willy A. Bachofen AG) by established methods (King and Kunji, 2020).

Preparation of lipid for protein purification

Tetraoleoyl cardiolipin (18:1) powder was purchased from Avanti Polar Lipids. Lipids were solubilized in 10% (w/v) lauryl maltose neopentyl glycol (Anatrace) by vortexing for 4 hours at room temperature to give 10 mg mL^{-1} lipid in a 10% (w/v) detergent stock. The stocks were stored in liquid nitrogen.

Protein purification by nickel affinity chromatography

Protein was purified as described previously for the human mitochondrial ADP/ATP carrier (Jaiquel Baron et al., 2021). In total, 0.5 g of mitochondria were solubilized in 1.5% (w/v) lauryl maltose neopentyl glycol, protease inhibitor tablet (Roche), 20 mM imidazole, and 150 mM NaCl for one hour by rotation at 4 °C. The insoluble material was separated from the soluble fraction by centrifugation (200,000 *g*, 45 minutes, 4 °C). Nickel Sepharose slurry (0.5 mL resin; GE healthcare) was added to the soluble fraction; the mixture was stirred at 4 °C for one hour. The nickel resin was harvested by centrifugation (100 *g*, 10 minutes, 4 °C), transferred to a Proteus 1-step batch midi spin column (Generon), and washed with 40 column volumes of buffer A (20 mM HEPES pH 7.0, 150 mM NaCl, 40 mM imidazole, 0.1 mg mL^{-1} tetraoleoyl cardiolipin / 0.1% (w/v) lauryl maltose neopentyl glycol) (100 *g*, 5 minutes, 4 °C); followed by 10 column volumes of buffer B (20 mM HEPES pH 7.0, 50 mM NaCl, 0.1 mg mL^{-1}

tetraoleoyl cardiolipin / 0.1% (w/v) lauryl maltose neopentyl glycol) (100 *g*, 5 minutes, 4 °C). The nickel resin was resuspended in buffer B and incubated with 10 mM imidazole, 20 µg factor Xa protease (NEB) and 5 mM $CaCl_2$ with inversion at 10 °C overnight. Protein was eluted by centrifugation on a spin column (100 *g*, 2 minutes, 4 °C). Imidazole and NaCl were removed using a PD-10 desalting column according to the manufacturer's instructions (GE Healthcare) at 4 °C and the concentration was determined by spectrometry (NanoDrop Technologies) at 280 nm using calculated extinction coefficients (hOGC: 29,000 M^{-1} cm^{-1}; hDIC: 20,900 M^{-1} cm^{-1}; bOGC: 50,350 M^{-1} cm^{-1}; bGIC-1: 48,735 M^{-1} cm^{-1}; bGIC-2: 41,620 M^{-1} cm^{-1}).

Generation and testing of antibodies

Specific peptides (C+LSGEGTSEKLYSSSF for bOGC, C+IVAPGEARLGSIKMA for bGIC-1 and C+TAAEGRISGMAIAKS for bGIC-2) were generated as a N-terminal *Keyhole limpet* haemocyanin fusion to raise the antibodies in rabbits (Eurogentec). For Western blots, an overnight incubation with 1:2,000 α-bOGC, 1:6,000 α-bGIC1, and 1:1,000 α-bGIC2 and one hour incubation with secondary 1:20,000 goat α-rabbit-HRP (Millipore) against 100 ng of purified protein was used. The membranes were developed with ECL Western Blotting Detection Reagents (Amersham).

Cell culture

Axenic cultures of *Blastocystis* ST7-B were a generous gift from Professor Kevin S. W. Tan (National University of Singapore) and were grown as described previously (Leonardi et al., 2021).

Confocal microscopy

Blastocystis ST7-B cells were harvested by centrifugation (1,000 *g*, 10 minutes) at ambient temperature. Cells were washed with pre-reduced PBS, and fixed with 4% methanol-free formaldehyde (Thermo Fisher Scientific), incubated at 37 °C for 30 minutes. Fixed parasites were permeabilized with 0.1% Triton X-100, and blocked with 3% BSA prior to antibody staining. Rabbit antibodies against bGIC-1 , bGIC-2 , and bOGC (Eurogentec) were diluted with 3% BSA in PBS with 0.01% Triton X-100 at 1:5000, 1:1000, and 1:1500, respectively, and incubated overnight at 4 °C. Guinea pig anti-TPI-GAPDH (1:1000; Eurogentec), previously shown to localise in the mitochondria (Bártulos et al., 2018) was used as an mitochondrial marker. Alexa

Fluor™ 488 conjugated goat anti-rabbit (A-21428, Invitrogen) and Alexa Fluor™ 555 conjugated goat anti-guinea pig (A-11073, Invitrogen), used as secondary antibodies, were diluted with 3% BSA in PBS with 0.01% Triton X-100 at 0.5 µg mL^{-1} and 2 µg mL^{-1}, respectively. Hoechst 33342 (5 µg mL^{-1}, Thermo Fisher Scientific) was used to stain DNA. All immunofluorescence assays were carried out in No. 1.5 high precision glass cover slips (Marienfeld) coated with 20 µg Cell-Tak (Corning). Cells were mounted using ProLong™ Gold Antifade Mountant (Molecular Probes) and cured overnight. Images were taken using a Leica SP8 laser scanning confocal microscope (Leica Microsystems) equipped with oil immersion objective lens (Leica Microsystems, HC PL APO CS2 100x/1.40 NA). Z-stacks were collected with a system-optimized sampling compliant to the Nyquest-Shannon sampling theorem and with LAS X LIGHTNING deconvolution-optimized settings (Leica Microsystems). Optical sections from the image stacks were further processed using Fiji Version 1.54d.

Thermostability analysis

Thermal unfolding analyses were performed with dye-free differential scanning fluorimetry (nanoDSF), which monitors the changes in the spectral properties of tryptophan and tyrosine residues due to changes in their environment caused by unfolding (Alexander et al., 2014). The proteins have the following number of tryptophans: hOGC (two); hDIC (one); bOGC (five); bGIC-1 (five); bGIC-2 (four). Approximately 0.6 µg of protein and 10 mM substrate were added into a final volume of 10 µL purification buffer B, and the samples were loaded into nanoDSF-grade standard glass capillaries. The temperature was increased by 4 °C every minute from 25 to 95 °C, the intrinsic fluorescence was measured in a Prometheus NT.48 nanoDSF device, and the apparent melting temperature (Tm) was calculated with the PR.ThermControl software (NanoTemper Technologies).

Reconstitution of carrier protein into liposomes

A mix containing *Escherichia coli* polar lipid extract (Avanti Polar Lipids order number: 100600C), egg L-α-phosphatidylcholine (Avanti Polar Lipids order number: 840051C) and tetraoleoyl cardiolipin (Avanti Polar Lipids order number: 710335C) in a 15:5:1 (w/w) ratio was dried under a stream of nitrogen: 6.3 mg of total lipids were used per sample (0.625 mL). Lipids were re-hydrated in 20 mM HEPES pH 7.0, 50

mM NaCl and 5 mM $MgCl_2$. The detergent pentaethylene glycol monodecyl ether ($C_{10}E_5$) was added to a final concentration of 2.5% (v/v), and the lipids were solubilized by vortexing and incubated on ice: the equivalent 30 µg protein was added per sample. The pentaethylene glycol monodecyl was removed by SM-2 bio-beads (Bio-Rad): five additions of bio-beads were made to the master mix every 20 minutes with inversion at 4 °C: four additions of 30 mg, and the final addition of 240 mg per sample. The samples were incubated overnight at 4 °C with rotation. Bio-beads were removed by passage through empty micro-bio spin columns (Bio-Rad). The compound was internalized by freeze-thaw-extrusion (Jaiquel Baron et al., 2021). Compound, to a final concentration of 5 mM (malate and sulphate assays) or 10 mM (phosphate assays) was added, and the sample was subjected to three cycles of freezing in liquid nitrogen for two minutes followed by thawing in a room temperature water bath for ten minutes. Proteoliposomes were subsequently extruded by 21 passages through a 0.4-µm filter (Millipore), and the external substrate was removed and exchanged into buffer (20 mM HEPES, pH 7.0 and 50 mM NaCl) using a PD10 desalting column (GE Healthcare) according to manufacturer's instructions.

Transport assays

Transport assays were performed using the Hamilton MicroLab Star robot (Hamilton Robotics Ltd). Proteoliposomes (100 µL) were loaded into the wells of a MultiScreenHTS + HA 96-well filter plate (pore size 0.45-µm, Millipore). Uptake of the radiolabelled substrate was initiated by the addition of 100 µL buffer containing 2.5 µM [^{14}C]-malate (American Radiolabelled Chemicals), 25 µM [^{35}S]-sodium sulphate (Hartmann Analytic), or 200 µM [^{33}P]-orthophosphoric acid (Hartmann Analytic). Uptake was stopped after 0, 10, 20, 30, 45, 60, 150, 300, 450 and 600 seconds by filtration and washing three times with 200 µL ice-cold buffer (20 mM HEPES, pH 7.0, 50 mM NaCl). Plates were dried overnight, 200 µL MicroScint-20 (Perkin Elmer) were added, and levels of radioactivity were determined using a TopCount scintillation counter (Perkin Elmer). Initial rates were determined from the linear part of the uptake curve (60 seconds).

SDS-PAGE analysis and protein quantification

Protein was visualized by SDS-PAGE analysis using 4-12% bis-tris mPAGE gels and stained using InstantBlue (Abcam), according to the manufacturer's instructions. Reconstitution efficiency was determined by comparing the amount of protein incorporated into proteoliposome samples to a standard curve of known amounts of purified protein.

Acknowledgements

MSK and ACK were supported by grant MC_UU_00028/2 of the UK Medical Research Council to ERSK, and EP and MRT were supported by Norwegian Research Council grant 301170 to MvdG. We thank Dr. Shane Palmer (MRC Mitochondrial Biology Unit) for carrying out large-scale fermentations in this project, Drs. Denis Lacabanne, Sotiria Tavoulari, Camila Cimadamore-Werthein and Pavel Dolezal for constructive comments on the manuscript, and Associate Professor Kevin S. W. Tan for the ST7-B *Blastocystis* culture.

Author contributions

Conception and design of the research: E.P., M.S.K., M.v.d.G., and E.R.S.K.
Bioinformatic analyses: A.C.K. and E.P.
Molecular biology: M.S.K.
Microscopy: M.R.T.
Protein purification and thermostability analyses: E.P.
Transport assays: E.P., and M.S.K.
Data analysis: E.P. and M.S.K.
Data interpretation: E.P., M.S.K., M.v.d.G., and E.R.S.K.
Writing of the paper: E.P., M.S.K., A.C.K., M.R.T., M.v.d.G., and E.R.S.K
All authors read and revised the paper.

Competing financial interests

The authors declare no competing interests.

References

Abrahamian, M., Kagda, M., Ah-Fong, A.M.V., and Judelson, H.S. (2017). Rethinking the evolution of eukaryotic metabolism: novel cellular partitioning of enzymes in stramenopiles links serine biosynthesis to glycolysis in mitochondria. BMC Evol Biol *17*, 241.

Ajjampur, S.S., Png, C.W., Chia, W.N., Zhang, Y., and Tan, K.S. (2016). Ex Vivo and In Vivo Mice Models to Study Blastocystis spp. Adhesion, Colonization and Pathology: Closer to Proving Koch's Postulates. PLoS One *11*, e0160458.

Alexander, C.G., Wanner, R., Johnson, C.M., Breitsprecher, D., Winter, G., Duhr, S., Baaske, P., and Ferguson, N. (2014). Novel microscale approaches for easy, rapid determination of protein stability in academic and commercial settings. Biochim Biophys Acta *1844*, 2241-2250.

Andersen, L.O., Bonde, I., Nielsen, H.B., and Stensvold, C.R. (2015). A retrospective metagenomics approach to studying Blastocystis. FEMS Microbiol Ecol *91*.

Andersen, L.O., and Stensvold, C.R. (2016). Blastocystis in Health and Disease: Are We Moving from a Clinical to a Public Health Perspective? J Clin Microbiol *54*, 524-528.

Audebert, C., Even, G., Cian, A., Blastocystis Investigation, G., Loywick, A., Merlin, S., Viscogliosi, E., and Chabe, M. (2016). Colonization with the enteric protozoa Blastocystis is associated with increased diversity of human gut bacterial microbiota. Sci Rep *6*, 25255.

Bártulos, R.C., Rogers, M.B., Williams, T.A., Gentekaki, E., Brinkmann, H., Cerff, R., Liaud, M.F., Hehl, A.B., Yarlett, N.R., Gruber, A.*, et al.* (2018). Mitochondrial Glycolysis in a Major Lineage of Eukaryotes. Genome Biol Evol *10*, 2310-2325.

Bisaccia, F., Indiveri, C., and Palmieri, F. (1988). Purification and reconstitution of two anion carriers from rat liver mitochondria: the dicarboxylate and the 2-oxoglutarate carrier. Biochim Biophys Acta *933*, 229-240.

Bricker, D.K., Taylor, E.B., Schell, J.C., Orsak, T., Boutron, A., Chen, Y.C., Cox, J.E., Cardon, C.M., Van Vranken, J.G., Dephoure, N.*, et al.* (2012). A mitochondrial pyruvate carrier required for pyruvate uptake in yeast, Drosophila, and humans. Science *337*, 96-100.

Bruno, S., Pinto, A., Paredi, G., Tamborini, L., De Micheli, C., La Pietra, V., Marinelli, L., Novellino, E., Conti, P., and Mozzarelli, A. (2014). Discovery of covalent inhibitors of glyceraldehyde-3-phosphate dehydrogenase, a target for the treatment of malaria. J Med Chem *57*, 7465-7471.

Burki, F., Roger, A.J., Brown, M.W., and Simpson, A.G.B. (2020). The New Tree of Eukaryotes. Trends Ecol Evol *35*, 43-55.

Castegna, A., Scarcia, P., Agrimi, G., Palmieri, L., Rottensteiner, H., Spera, I., Germinario, L., and Palmieri, F. (2010). Identification and functional characterization of a novel mitochondrial carrier for citrate and oxoglutarate in *Saccharomyces cerevisiae*. J Biol Chem *285*, 17359-17370.

Crichton, P.G., Lee, Y., Ruprecht, J.J., Cerson, E., Thangaratnarajah, C., King, M.S., and Kunji, E.R. (2015). Trends in thermostability provide information on the nature of substrate, inhibitor, and lipid interactions with mitochondrial carriers. J Biol Chem *290*, 8206-8217.

Crompton, M., Palmieri, F., Capano, M., and Quagliariello, E. (1974). The transport of thiosulphate in rat liver mitochondria. FEBS Lett *46*, 247-250.

Deng, L., Lee, J.W.J., and Tan, K.S.W. (2022). Infection with pathogenic Blastocystis ST7 is associated with decreased bacterial diversity and altered gut microbiome profiles in diarrheal patients. Parasit Vectors *15*, 312.

Deng, L., Wojciech, L., Png, C.W., Kioh, D.Y.Q., Gu, Y., Aung, T.T., Malleret, B., Chan, E.C.Y., Peng, G., Zhang, Y.*, et al.* (2023). Colonization with two different Blastocystis subtypes in DSS-induced colitis mice is associated with strikingly different microbiome and pathological features. Theranostics *13*, 1165-1179.

Denoeud, F., Roussel, M., Noel, B., Wawrzyniak, I., Da Silva, C., Diogon, M., Viscogliosi, E., Brochier-Armanet, C., Couloux, A., Poulain, J.*, et al.* (2011). Genome sequence of the stramenopile Blastocystis, a human anaerobic parasite. Genome Biol *12*, R29.

Dogruman-Al, F., Kustimur, S., Yoshikawa, H., Tuncer, C., Simsek, Z., Tanyuksel, M., Araz, E., and Boorom, K. (2009). Blastocystis subtypes in irritable bowel syndrome and inflammatory bowel disease in Ankara, Turkey. Mem Inst Oswaldo Cruz *104*, 724-727.

Fiermonte, G., Dolce, V., Palmieri, L., Ventura, M., Runswick, M.J., Palmieri, F., and Walker, J.E. (2001). Identification of the human mitochondrial oxodicarboxylate carrier. Bacterial expression, reconstitution, functional characterization, tissue distribution, and chromosomal location. J Biol Chem *276*, 8225-8230.

Fiermonte, G., Walker, J.E., and Palmieri, F. (1993). Abundant bacterial expression and reconstitution of an intrinsic membrane-transport protein from bovine mitochondria. Biochem J *294*, 293-299.

673 Gentekaki, E., Curtis, B.A., Stairs, C.W., Klimes, V., Elias, M., Salas-Leiva, D.E., Herman, E.K.,
674 Eme, L., Arias, M.C., Henrissat, B., *et al.* (2017). Extreme genome diversity in the hyper-
675 prevalent parasitic eukaryote Blastocystis. PLoS Biol *15*, e2003769.
676 Haresh, K., Suresh, K., Khairul Anus, A., and Saminathan, S. (1999). Isolate resistance of
677 Blastocystis hominis to metronidazole. Trop Med Int Health *4*, 274-277.
678 Herzig, S., Raemy, E., Montessuit, S., Veuthey, J.L., Zamboni, N., Westermann, B., Kunji, E.R.,
679 and Martinou, J.C. (2012). Identification and functional expression of the mitochondrial
680 pyruvate carrier. Science *337*, 93-96.
681 Hoang, D.T., Chernomor, O., von Haeseler, A., Minh, B.Q., and Vinh, L.S. (2018). UFBoot2:
682 Improving the Ultrafast Bootstrap Approximation. Mol Biol Evol *35*, 518-522.
683 Jaiquel Baron, S., King, M.S., Kunji, E.R.S., and Schirris, T.J.J. (2021). Characterization of drug-
684 induced human mitochondrial ADP/ATP carrier inhibition. Theranostics *11*, 5077-5091.
685 Jiang, R.H., and Tyler, B.M. (2012). Mechanisms and evolution of virulence in oomycetes.
686 Annu Rev Phytopathol *50*, 295-318.
687 Jones, P., Binns, D., Chang, H.Y., Fraser, M., Li, W., McAnulla, C., McWilliam, H., Maslen, J.,
688 Mitchell, A., Nuka, G., *et al.* (2014). InterProScan 5: genome-scale protein function
689 classification. Bioinformatics *30*, 1236-1240.
690 King, M.S., and Kunji, E.R.S. (2020). Expression and purification of membrane proteins in
691 *Saccharomyces cerevisiae*. Methods Mol Biol *2127*, 47-61.
692 Kunji, E.R.S., King, M.S., Ruprecht, J.J., and Thangaratnarajah, C. (2020). The SLC25 Carrier
693 Family: Important Transport Proteins in Mitochondrial Physiology and Pathology. Physiology
694 (Bethesda) *35*, 302-327.
695 Kunji, E.R.S., and Robinson, A.J. (2006). The conserved substrate binding site of
696 mitochondrial carriers. Biochim Biophys Acta *1757*, 1237-1248.
697 Lantsman, Y., Tan, K.S.W., Morada, M., and Yarlett, N. (2008). Biochemical characterization
698 of a mitochondrial-like organelle from Blastocystis sp. subtype 7. Microbiology (Reading)
699 *154*, 2757-2766.
700 Leonardi, S.S., Li, F.J., Chee, M.S., Yason, J.A., Tay, H.Y., Chen, J.Y., Koh, E.Y., He, C.Y., and
701 Tan, K.S. (2021). Characterisation of novel functionality within the Blastocystis
702 tryptophanase gene. PLoS Negl Trop Dis *15*, e0009730.

Majd, H., King, M.S., Palmer, S.M., Smith, A.C., Elbourne, L.D., Paulsen, I.T., Sharples, D., Henderson, P.J., and Kunji, E.R. (2018). Screening of candidate substrates and coupling ions of transporters by thermostability shift assays. Elife *7*, e38821.

Mavridou, V., King, M.S., Tavoulari, S., Ruprecht, J.J., Palmer, S.M., and Kunji, E.R.S. (2022). Substrate binding in the mitochondrial ADP/ATP carrier is a step-wise process guiding the structural changes in the transport cycle. Nat Commun *13*, 3585.

McNae, I.W., Kinkead, J., Malik, D., Yen, L.H., Walker, M.K., Swain, C., Webster, S.P., Gray, N., Fernandes, P.M., Myburgh, E.*, et al.* (2021). Fast acting allosteric phosphofructokinase inhibitors block trypanosome glycolysis and cure acute African trypanosomiasis in mice. Nat Commun *12*, 1052.

Minh, B.Q., Schmidt, H.A., Chernomor, O., Schrempf, D., Woodhams, M.D., von Haeseler, A., and Lanfear, R. (2020). IQ-TREE 2: New Models and Efficient Methods for Phylogenetic Inference in the Genomic Era. Mol Biol Evol *37*, 1530-1534.

Mirza, H., Teo, J.D., Upcroft, J., and Tan, K.S. (2011). A rapid, high-throughput viability assay for Blastocystis spp. reveals metronidazole resistance and extensive subtype-dependent variations in drug susceptibilities. Antimicrob Agents Chemother *55*, 637-648.

Moghaddam, D.D., Ghadirian, E., and Azami, M. (2005). Blastocystis hominis and the evaluation of efficacy of metronidazole and trimethoprim/sulfamethoxazole. Parasitol Res *96*, 273-275.

Müller, M., Mentel, M., van Hellemond, J.J., Henze, K., Woehle, C., Gould, S.B., Yu, R.Y., van der Giezen, M., Tielens, A.G., and Martin, W.F. (2012). Biochemistry and evolution of anaerobic energy metabolism in eukaryotes. Microbiol Mol Biol Rev *76*, 444-495.

Nakayama, T., Ishida, K., and Archibald, J.M. (2012). Broad distribution of TPI-GAPDH fusion proteins among eukaryotes: evidence for glycolytic reactions in the mitochondrion? PLoS One *7*, e52340.

Opperdoes, F.R., and Borst, P. (1977). Localization of nine glycolytic enzymes in a microbody-like organelle in Trypanosoma brucei: the glycosome. FEBS Lett *80*, 360-364.

Palmieri, F., Quagliariello, E., and Klingenberger, M. (1972). Kinetics and specificity of the oxoglutarate carrier in rat-liver mitochondria. Eur J Biochem *29*, 408-416.

Penna-Coutinho, J., Cortopassi, W.A., Oliveira, A.A., Franca, T.C., and Krettli, A.U. (2011). Antimalarial activity of potential inhibitors of Plasmodium falciparum lactate dehydrogenase enzyme selected by docking studies. PLoS One *6*, e21237.

735 Picault, N., Palmieri, L., Pisano, I., Hodges, M., and Palmieri, F. (2002). Identification of a
736 novel transporter for dicarboxylates and tricarboxylates in plant mitochondria. Bacterial
737 expression, reconstitution, functional characterization, and tissue distribution. J Biol Chem
738 *277*, 24204-24211.
739 Poirier, P., Wawrzyniak, I., Vivares, C.P., Delbac, F., and El Alaoui, H. (2012). New insights into
740 Blastocystis spp.: a potential link with irritable bowel syndrome. PLoS Pathog *8*, e1002545.
741 Priyam, A., Woodcroft, B.J., Rai, V., Moghul, I., Munagala, A., Ter, F., Chowdhary, H., Pieniak,
742 I., Maynard, L.J., Gibbins, M.A.*, et al.* (2019). Sequenceserver: A Modern Graphical User
743 Interface for Custom BLAST Databases. Mol Biol Evol *36*, 2922-2924.
744 Ravindra, G., and Balaram, P. (2005). Plasmodium falciparum triosephosphate isomerase:
745 New insights into an old enzyme. Pure Appl Chem *77*, 281-289.
746 Robinson, A.J., and Kunji, E.R.S. (2006). Mitochondrial carriers in the cytoplasmic state have
747 a common substrate binding site. Proc Natl Acad Sci USA *103*, 2617-2622.
748 Ruprecht, J.J., King, M.S., Zogg, T., Aleksandrova, A.A., Pardon, E., Crichton, P.G., Steyaert, J.,
749 and Kunji, E.R.S. (2019). The molecular mechanism of transport by the mitochondrial
750 ADP/ATP carrier. Cell *176*, 435-447.
751 Ruprecht, J.J., and Kunji, E.R.S. (2020). The SLC25 mitochondrial carrier family: structure and
752 mechanism. Trends Biochem Sci *45*, 244-258.
753 Ruprecht, J.J., and Kunji, E.R.S. (2021). Structural Mechanism of Transport of Mitochondrial
754 Carriers. Annu Rev Biochem *90*, 535-558.
755 Saraste, M., and Walker, J.E. (1982). Internal sequence repeats and the path of polypeptide
756 in mitochondrial ADP/ATP translocase. FEBS Lett *144*, 250-254.
757 Saris, N.E.L. (1980). Sulfate transport by H+ symport and by the dicarboxylate carrier in
758 mitochondria. Biochem J *192*, 911-917.
759 Stechmann, A., Hamblin, K., Perez-Brocal, V., Gaston, D., Richmond, G.S., van der Giezen, M.,
760 Clark, C.G., and Roger, A.J. (2008). Organelles in Blastocystis that blur the distinction
761 between mitochondria and hydrogenosomes. Curr Biol *18*, 580-585.
762 Stensvold, C.R., Berg, R., Maloney, J.G., Molokin, A., and Santin, M. (2023). Molecular
763 characterization of *Blastocystis* and *Entamoeba* of muskoxen and sheep in Greenland. Int J
764 Parasitol *53*, 673-685.
765 Stensvold, C.R., Lewis, H.C., Hammerum, A.M., Porsbo, L.J., Nielsen, S.S., Olsen, K.E.,
766 Arendrup, M.C., Nielsen, H.V., and Molbak, K. (2009). Blastocystis: unravelling potential risk

767 factors and clinical significance of a common but neglected parasite. Epidemiol Infect *137*,
768 1655-1663.
769 Stensvold, C.R., Sorland, B.A., Berg, R., Andersen, L.O., van der Giezen, M., Bowtell, J.L., El-
770 Badry, A.A., Belkessa, S., Kurt, O., and Nielsen, H.V. (2022). Stool Microbiota Diversity
771 Analysis of Blastocystis-Positive and Blastocystis-Negative Individuals. Microorganisms *10*.
772 Stensvold, C.R., and van der Giezen, M. (2018). Associations between Gut Microbiota and
773 Common Luminal Intestinal Parasites. Trends Parasitol *34*, 369-377.
774 Stenzel, D.J., and Boreham, P.F. (1996). Blastocystis hominis revisited. Clin Microbiol Rev *9*,
775 563-584.
776 Tavoulari, S., Schirris, T.J.J., Mavridou, V., Thangaratnarajah, C., King, M.S., Jones, D.T.D.,
777 Ding, S., Fearnley, I.M., and Kunji, E.R.S. (2022). Key features of inhibitor binding to the
778 human mitochondrial pyruvate carrier hetero-dimer. Mol Metab, 101469.
779 Tito, R.Y., Chaffron, S., Caenepeel, C., Lima-Mendez, G., Wang, J., Vieira-Silva, S., Falony, G.,
780 Hildebrand, F., Darzi, Y., Rymenans, L.*, et al.* (2019). Population-level analysis of Blastocystis
781 subtype prevalence and variation in the human gut microbiota. Gut *68*, 1180-1189.
782 Toleco, M.R., Naake, T., Zhang, Y., Heazlewood, J.L., and Fernie, A.R. (2020). Plant
783 Mitochondrial Carriers: Molecular Gatekeepers That Help to Regulate Plant Central Carbon
784 Metabolism. Plants (Basel) *9*.
785 Tsaousis, A.D., Hamblin, K.A., Elliott, C.R., Young, L., Rosell-Hidalgo, A., Gourlay, C.W.,
786 Moore, A.L., and van der Giezen, M. (2018). The Human Gut Colonizer Blastocystis Respires
787 Using Complex II and Alternative Oxidase to Buffer Transient Oxygen Fluctuations in the Gut.
788 Front Cell Infect Microbiol *8*, 371.
789 Wawrzyniak, I., Roussel, M., Diogon, M., Couloux, A., Texier, C., Tan, K.S., Vivares, C.P.,
790 Delbac, F., Wincker, P., and El Alaoui, H. (2008). Complete circular DNA in the mitochondria-
791 like organelles of Blastocystis hominis. Int J Parasitol *38*, 1377-1382.
792 Wu, Z., Mirza, H., and Tan, K.S. (2014). Intra-subtype variation in enteroadhesion accounts
793 for differences in epithelial barrier disruption and is associated with metronidazole
794 resistance in Blastocystis subtype-7. PLoS Negl Trop Dis *8*, e2885.
795 Yason, J.A., Liang, Y.R., Png, C.W., Zhang, Y., and Tan, K.S.W. (2019). Interactions between a
796 pathogenic Blastocystis subtype and gut microbiota: in vitro and in vivo studies. Microbiome
797 *7*, 30.

Zhou, L., Maldonado, M., Padavannil, A., Guo, F., and Letts, J.A. (2022). Structures of Tetrahymena's respiratory chain reveal the diversity of eukaryotic core metabolism. Science *376*, 831-839.

Zierdt, C.H. (1991). Blastocystis hominis--past and future. Clin Microbiol Rev *4*, 61-79.

Zierdt, C.H., Donnolley, C.T., Muller, J., and Constantopoulos, G. (1988). Biochemical and ultrastructural study of Blastocystis hominis. J Clin Microbiol *26*, 965-970.

Figures and legends

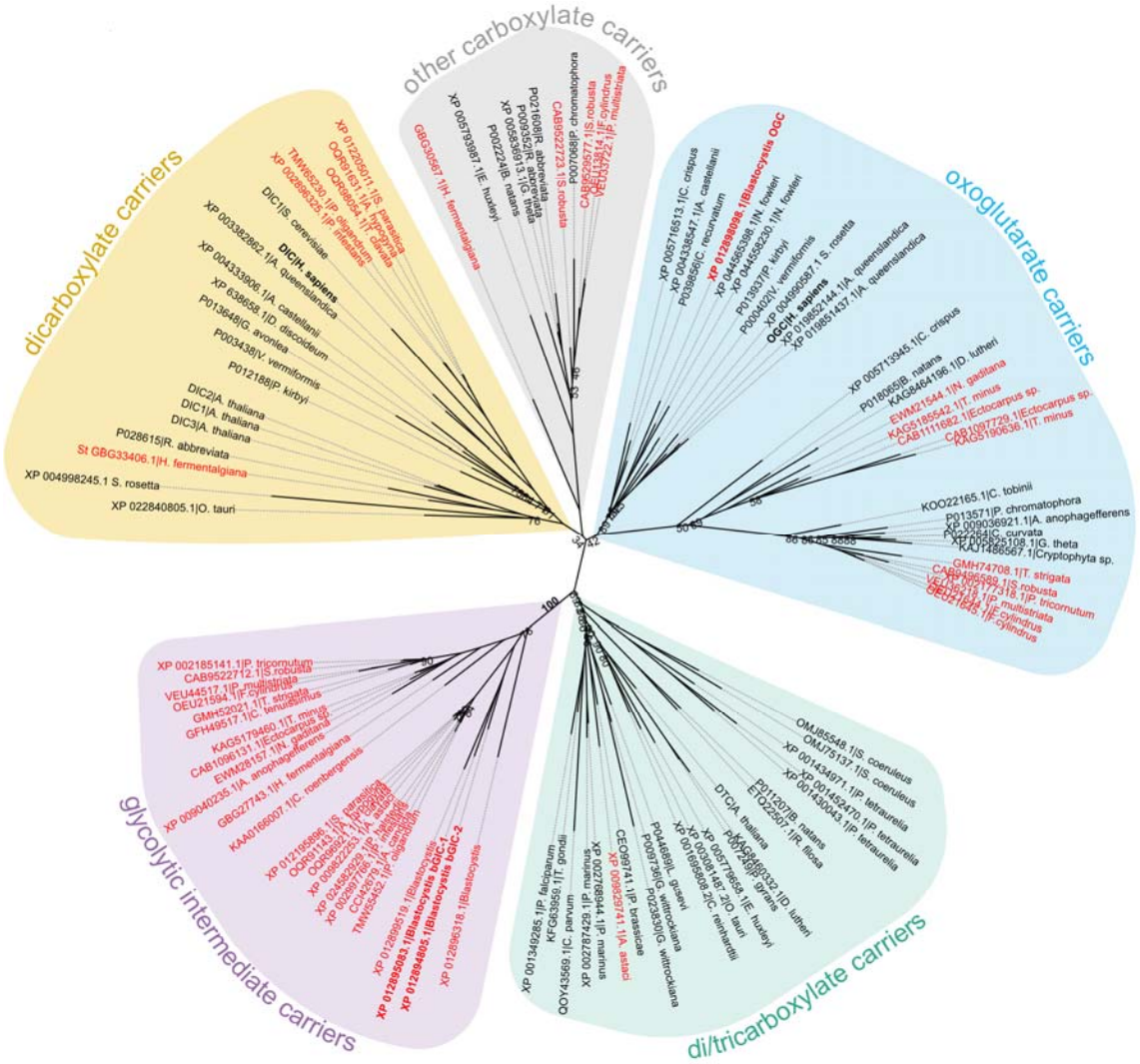

Figure 1: Phylogenetic analysis of carboxylate carriers. The maximum likelihood tree was generated by IQ-TREE with the LG + F + R7 model suggested by ModelFinder. The support was calculated using ultrafast bootstrap analysis. The unrooted phylogenetic tree shows the uniqueness of the identified putative stramenopile glycolytic intermediate carriers amongst eukaryotes. The stramenopile-specific glycolytic intermediate carriers (GIC - pink) are most closely related to di/tricarboxylate carriers (DTC – green), and to a lesser extend to oxoglutarate carriers (OGC - blue) and dicarboxylate carriers (DIC - yellow). Stramenopile proteins are in red, proteins included in this study are in bold. Note the absence of any non-

stramenopile sequences in this clade. Bootstrap values less than 90 and a value for the GIC group are indicated.

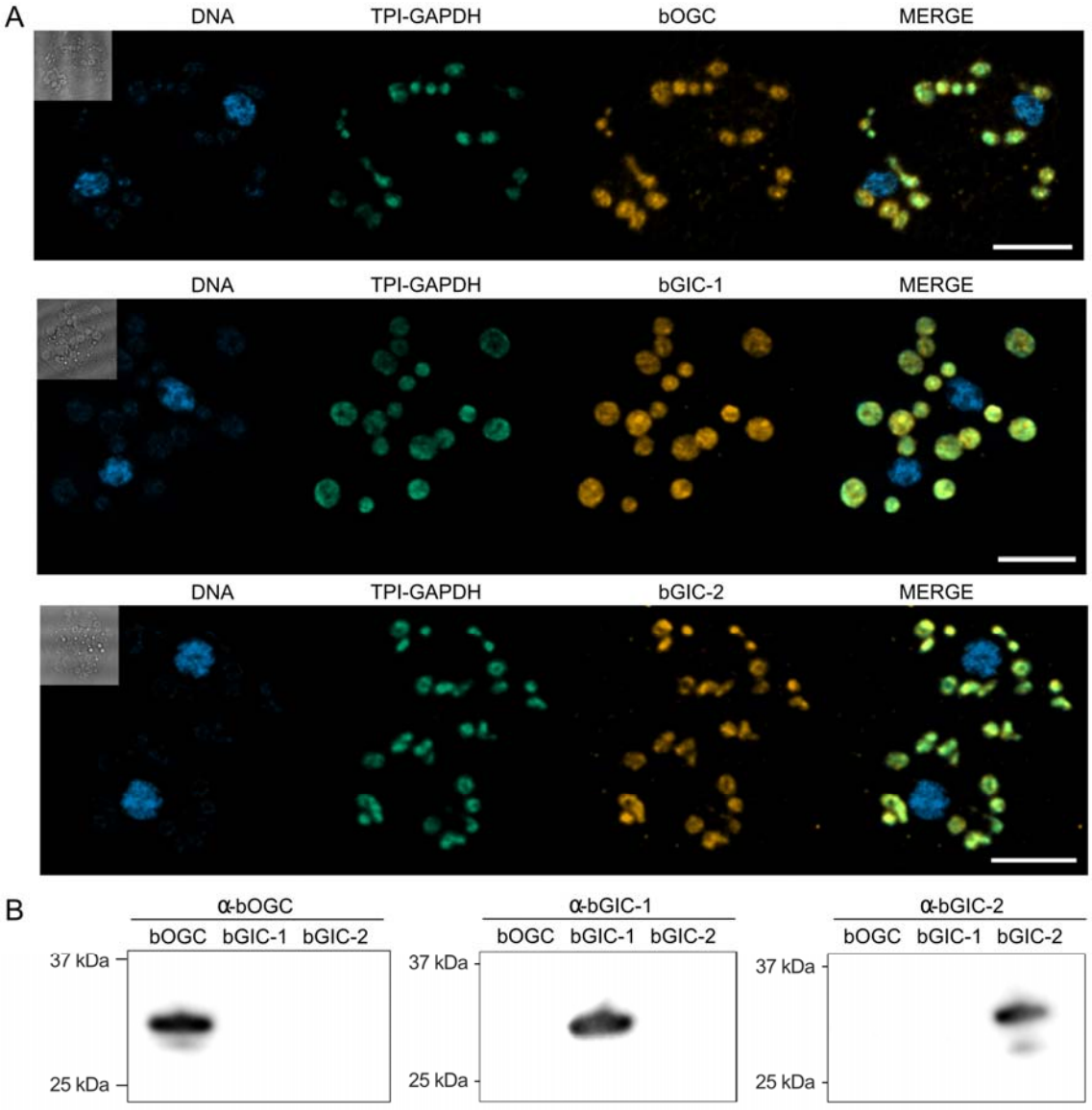

Figure 2: A) Localisation of GIC carriers in *Blastocystis* ST7-B cells using specific antibodies (orange). The signal colocalises with the mitochondrial protein TPI-GAPDH (green) (Bártulos et al., 2018), demonstrating its mitochondrial localisation. DNA is stained with Hoechst 33342 (blue). The scale bar is 5 µm. **B**) Western blots of *Blastocystis* OGC, GIC-1, and GIC-2 antibodies against purified protein confirm that there is no cross reactivity.

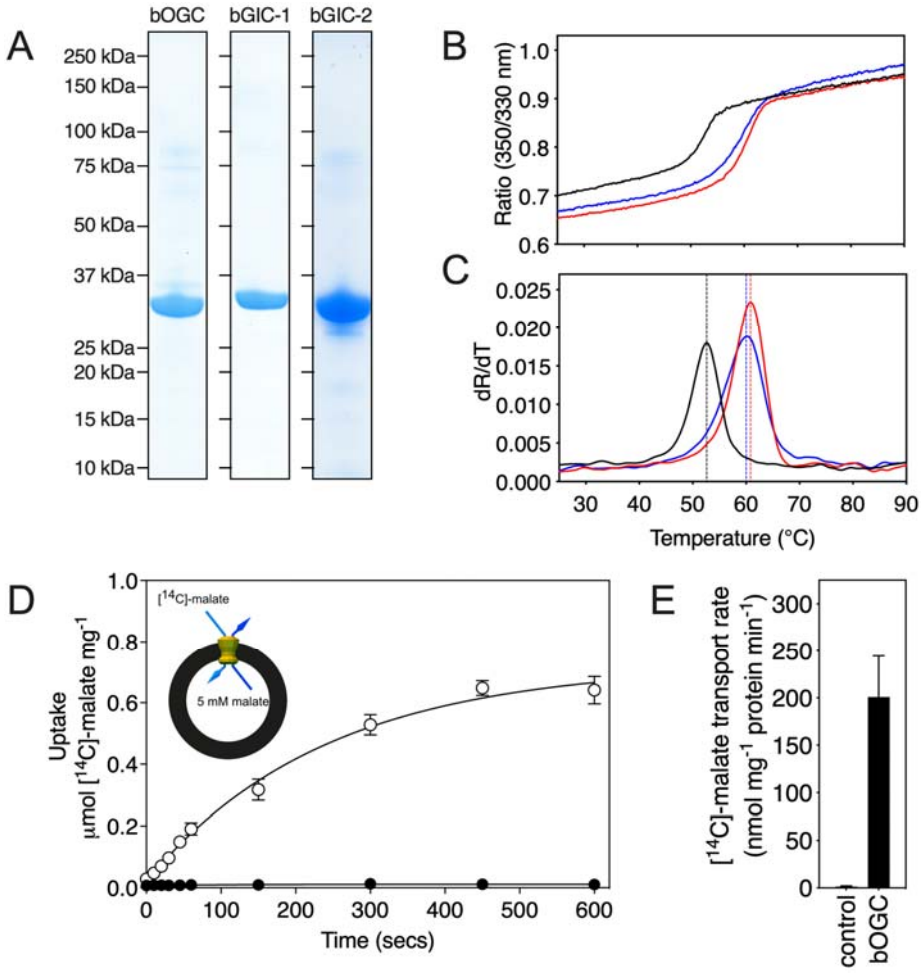

Figure 3: Expression, purification and biophysical characterization of *Blastocystis* carriers. **A**) Instant-blue stained SDS-PAGE gel of purified bOGC, bGIC-1 and bGIC-2. **B**) Typical unfolding curves of bOGC (black trace), bGIC-1 (red trace), and bGIC-2 (blue trace) using nanoDSF. **C**) The peak in the derivative of the unfolding curve (dR/dT) is the apparent melting temperature (Tm). **D**) [^{14}C]-malate uptake curve of bOGC reconstituted into proteoliposomes loaded with (white circles) or without (black circles) 5 mM malate. Transport was initiated by the external addition of 2.5 µM [^{14}C]-malate. **E**) Initial transport rates, calculated from panel **D**) from the linear part of the uptake curve (first 60 seconds). The data represent the mean and standard deviation is of n=4 (two biological repeats, each with two technical repeats).

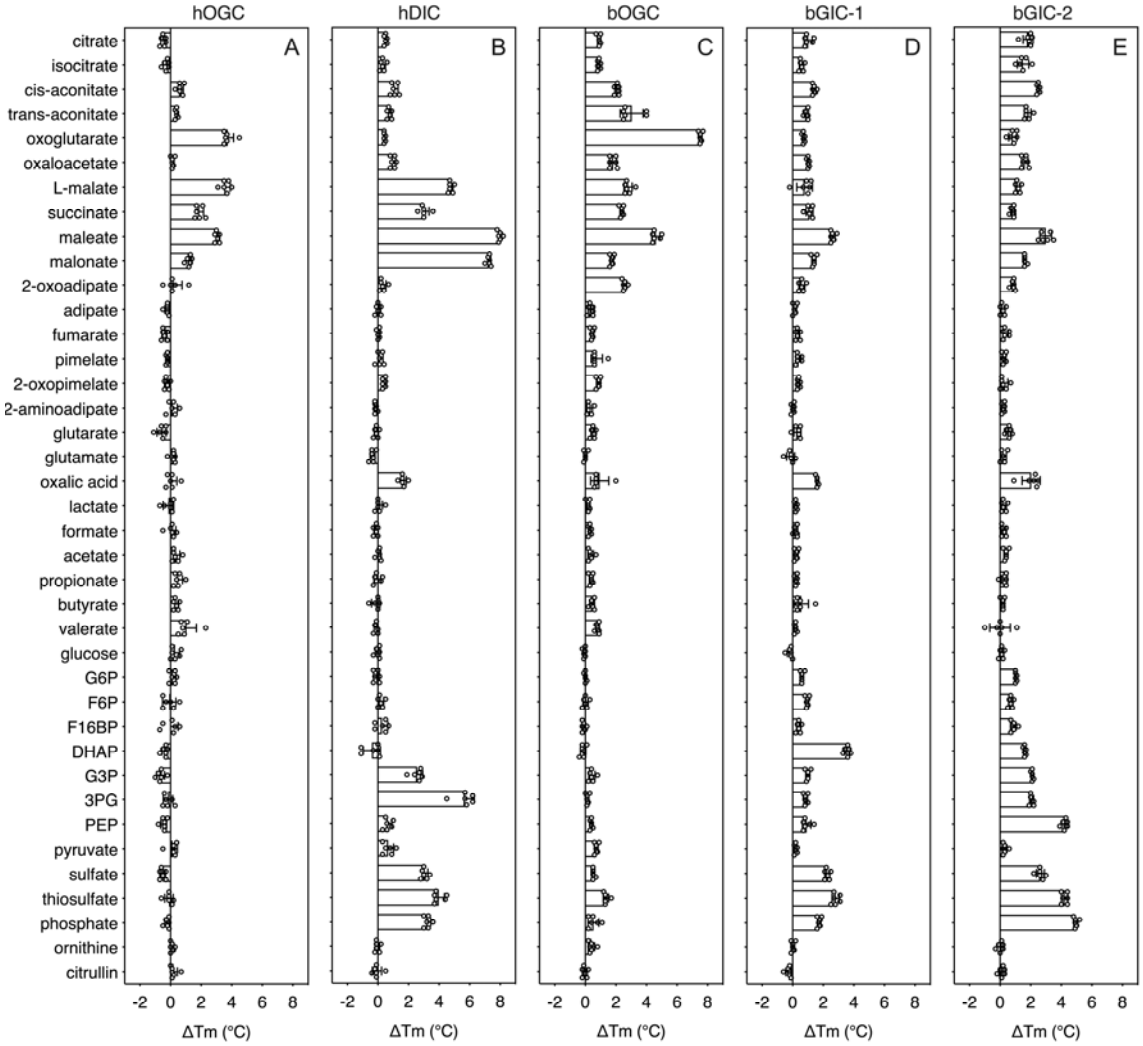

Figure 4: Thermostability screening of detergent-solubilized, purified protein using nanoDSF (Prometheus, Nanotemper). **A**) hOGC, **B**) hDIC, **C**) bOGC, **D**) bGIC-1, and **E**) bGIC-2 against 10 mM di- and tricarboxylates, glycolytic intermediates and inorganic ions. The temperature shift (ΔTm) is the apparent melting temperature in the presence of compound minus the apparent melting temperature in the absence of compound. The data are represented by the mean and standard deviation of two biological repeats, each in triplicate (n=6 in total). G6P, glucose-6-phosphate; F6P, fructose-6-phosphate; F16BP, fructose 1-6 bisphosphate; DHAP, dihydroxyacetone phosphate; G3P, glyceraldehyde-3-phosphate; 3PG, 3-phosphoglycerate; PEP, phosphoenolpyruvate.

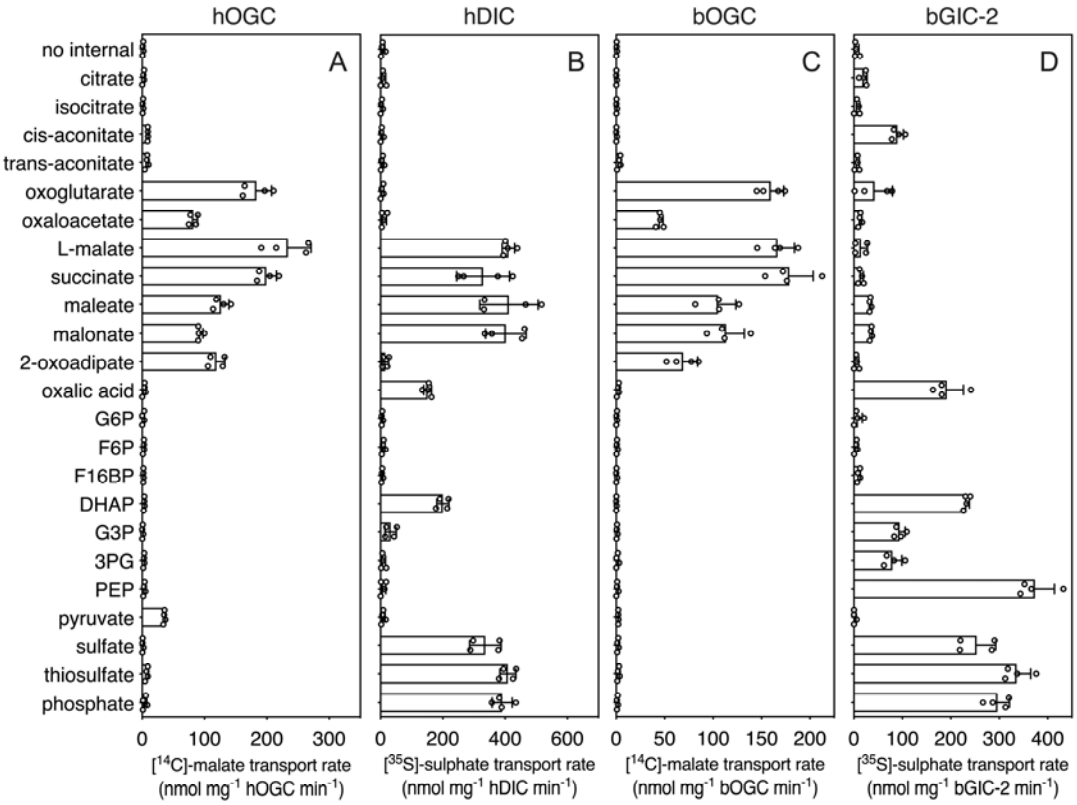

Figure 5: Hetero-exchange reactions catalysed by reconstituted carriers. **A**) Proteoliposomes containing human oxoglutarate carrier (hOGC, SLC25A11), **B**) human dicarboxylate carrier (hDIC, SLC25A10), **C**) *Blastocystis* oxoglutarate carrier (bOGC) and **D**) *Blastocystis* putative glycolytic intermediate carrier 2 (bGIC-2) were loaded with 5 mM compound, and transport initiated by the external addition of 2.5 µM [^{14}C]-malate (hOGC and bOGC) or 25 µM [^{35}S]-sulphate (hDIC and bGIC-2). Initial transport rates were calculated from the linear part of the uptake curve (60 seconds). The data represent the mean and standard deviation of two biological repeats, each with two technical repeats (n=4 in total). G6P, glucose-6-phosphate; F6P, fructose-6-phosphate; F16BP, fructose 1-6 bisphosphate; DHAP, dihydroxyacetone phosphate; G3P, glyceraldehyde-3-phosphate; 3PG, 3-phosphoglycerate; PEP, phosphoenolpyruvate.

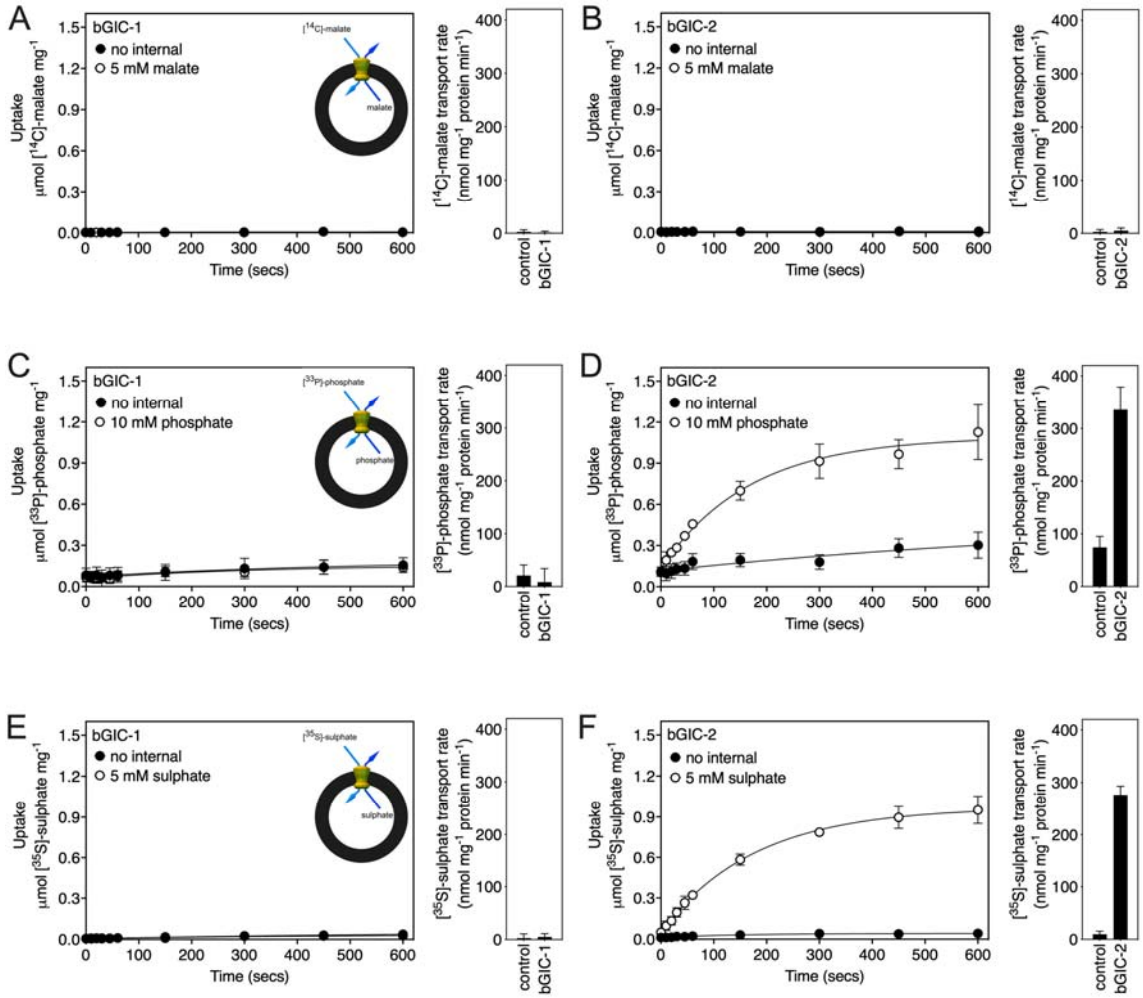

Figure 6: Proteoliposomes containing *Blastocystis* putative glycolytic intermediate carriers 1 (bGIC-1; **A**, **C** and **E**) and 2 (bGIC-2; **B**, **D** and **F**) were loaded with either (**A** and **B**) 5 mM malate, (**C** and **D**) 10 mM phosphate or (**E** and **F**) 5 mM sodium sulphate, and transport initiated by the external addition of (**A** and **B**) 2.5 µM [^{14}C]-malate, (**C** and **D**) 200 µM [^{33}P]-phosphate or (**E** and **F**) 25 µM [^{35}S]-sulphate. Controls with no internalized substrate were also tested (black circles). Initial transport rates were calculated from the linear part of the uptake curve (60 seconds). The data represent the mean and standard deviation of two biological repeats, each with two technical repeats (n=4 in total).

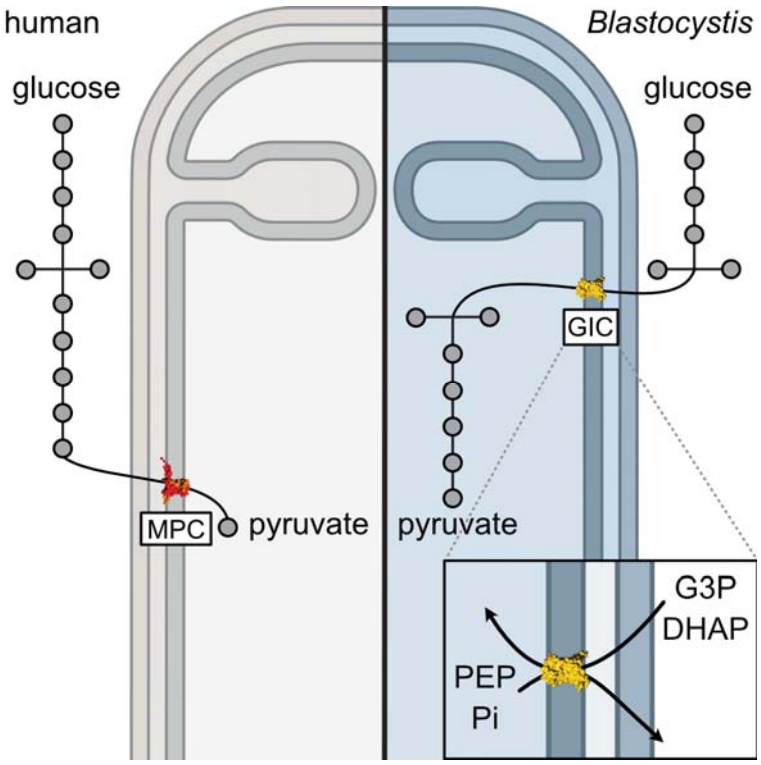

Figure 7: Comparing glycolysis in humans and *Blastocystis*.